ELSEVIER

Thermochimica Acta 391 (2002) 69–80

thermochimica acta

www.elsevier.com/locate/tca

Calibration of magnitude and phase angle of TMDSC Part 2. Calibration practice

M. Merzlyakov[a,1], G.W.H. Höhne[b], C. Schick[a,*]

[a]*FB Physik, University of Rostock, Universitätsplatz 3, 18051 Rostock, Germany*
[b]*Dutch Polymer Institute, Eindhoven University of Technology, P.O. Box 513, 5600 MB Eindhoven, The Netherlands*

Received 29 September 2001; received in revised form 29 January 2002; accepted 31 January 2002

Abstract

In the first part of this paper we have discussed the influence of heat transfer in temperature-modulated differential scanning calorimetry (TMDSC) and its influence on the measured signals, in particular, magnitude and phase angle of effective complex heat capacity. Fundamentals of transfer theory were given within the framework of linear response. On this basis different calibration methods were suggested which enable to correct the influence of heat transfer on the measured (effective) complex heat capacity in TMDSC. In the second part of the paper, we apply the different calibration methods to a single set of experimental data to compare the results with the expected ones, and to draw conclusion concerning the calibration method in question and the frequency range where the calibration algorithm works. The example has shown that the more simple calibration procedures lead to nearly the same uncertainties of the results in everyday measurements as the more sophisticated ''third order'' calibration procedure does. However, we recommend the ''third order'' calibration procedure in all cases where the heat transfer conditions could change during the measurement.

Keywords: TMDSC; Calibration; Complex heat capacity; Heat transfer; Correction

1. Introduction

In the first part of this paper [1], we presented the basis for the determination of the complex calibration function for the correction of the (complex) heat capacity measured with a temperature-modulated differential scanning calorimeter (TMDSC). The aim of the second part of this paper is to apply the different calibration algorithms presented in the first part [1] to a single set of experimental data, to compare the results with the expected ones, and to draw conclusion concerning the calibration method in question and the frequency range where the calibration algorithm works. To do so we apply the different calibration algorithms to a data set from a measurement from one instrument in a broad frequency range. We shall do that in different steps starting from rather simple calibration methods and proceeding to more complex methods which need more effort but enables the interested and more advanced user to come to better results. To understand better what follows, it would of course be helpful to study the first part of this paper first, but it is even possible to refrain from understanding the background and simply make use of the

* Corresponding author. Tel.: +49-381-498-1644; fax: +49-381-498-1626.
E-mail address: christoph.schick@physik.uni-rostock.de (C. Schick).
[1] Present address: Chemical Engineering, P.O. Box 43121, Texas Tech University, Lubbock, TX 79409, USA.

0040-6031/02/$ – see front matter
PII: S0040-6031(02)00164-8

recommended methods. However, we would like to summarize the considerations which the calibration methods are based on:

(i) The TMDSC is a linear device, and the behavior concerning the heat conduction can be described quantitatively with the tools of transfer theory. This can be done in time domain using either the pulse response (Greens) or the step response function, or in frequency domain using the complex transfer function (i.e. the normalized quotient of the output over the input function). All three functions are equivalent and can be converted into one another mathematically by integration, differentiation, and Fourier transform, respectively.
(ii) Linear response implies the possibility to breakdown a complex device into a network of simple elements with known transfer behavior. In the case of TMDSC the apparatus and the sample can be considered as connected in series, in other words the total transfer function is the product of the transfer function of the DSC and the transfer function of the sample. The simplest component is an *RC*-element with a certain thermal resistance R and a certain heat capacity C_p.

Most of the problems of proper calibration are related to heat transfer. The resulting changes of measured amplitude and phase angle of the heat flow rate appear most noticeably when large amounts of heat have to be exchanged and the thermal conductivity of the sample is low. A good example for such a situation would be polymer melting because of the large latent heat involved and the low thermal conductivity of polymers. Therefore, we should prove the different calibration algorithms just in the melting region of polymers. But there is no reference material available with well-known frequency dependent (complex) heat capacity in the melting region. We simply do not know which correct values one should expect there. For this reason, we chose the glass transition of a low thermal conducting polymer as an example for which the complex frequency dependent heat capacity is known. According to model calculations in the case of polystyrene (PS) [2], one expects a frequency dependence of the complex heat capacity as shown in Fig. 1.

Note that outside the glass transition region c_p^* is real valued (i.e. $\mathrm{Arg}(c_p^*) = 0$) and should be frequency independent. In the transition region the shape of c_p^* curves is step-like and more or less independent on modulation frequency, but with frequency increase by one decade the glass transition temperature T_g shifts about 3.5 K towards higher temperatures.

For the measurements, we took a rather large PS sample (25 mg) to force a larger influence of heat transfer to the sample. We used a Perkin Elmer Instruments Pyris 1 DSC with a block temperature of 5 °C, nitrogen purge, and standard aluminum pans of about 25 mg mass. We chose the multi-frequency approach [3] to generate the complex heat capacity spectrum of this material as a set of functions at discrete frequencies. Of course it is also possible to get the results in the common way, but in this case we have to perform a lot of single measurements at different frequencies which need much more time and—more important—there would be an increased scatter in heat capacity values from the varying measurements. We performed, however, two measurements with different basic periods of 20 and 3 min, respectively, in the temperature range 70–130 °C. The temperature–time profile was programmed by repeating isotherm and fast heating segments. The duration of the isotherm was 20 min for the first measurement and 3 min for the second measurement. The heating step was 2 K high with 150 K min^{-1} heating rate for both measurements, that made duration of the heating segment 0.8 s. For both measurements the (complex) effective heat capacity C_{eff}^* was calculated for a set of harmonics, resulting in two overlapping spectra. Then the two measurements were proved for compatibility: the magnitude and the phase angle of C_{eff}^* at 20th harmonic from the first measurement coincided with the magnitude and the phase angle of C_{eff}^* at third harmonic from the second measurement. Finally, the different calibration procedures were applied to these raw data.

As a criterion for the assessment of the quality of the calibration in question, we took a deviation from the expected value of 2% in magnitude and 0.02 rad in phase angle of C_{eff}^* as an acceptable limit of uncertainty. In fact, the limit concerning the phase angle is rather large, it is almost half of the total effect in phase angle for this sample, but the phase angle is really much more sensitive against heat transfer than the magnitude. The frequency where the heat capacity curves—corrected with the given calibration

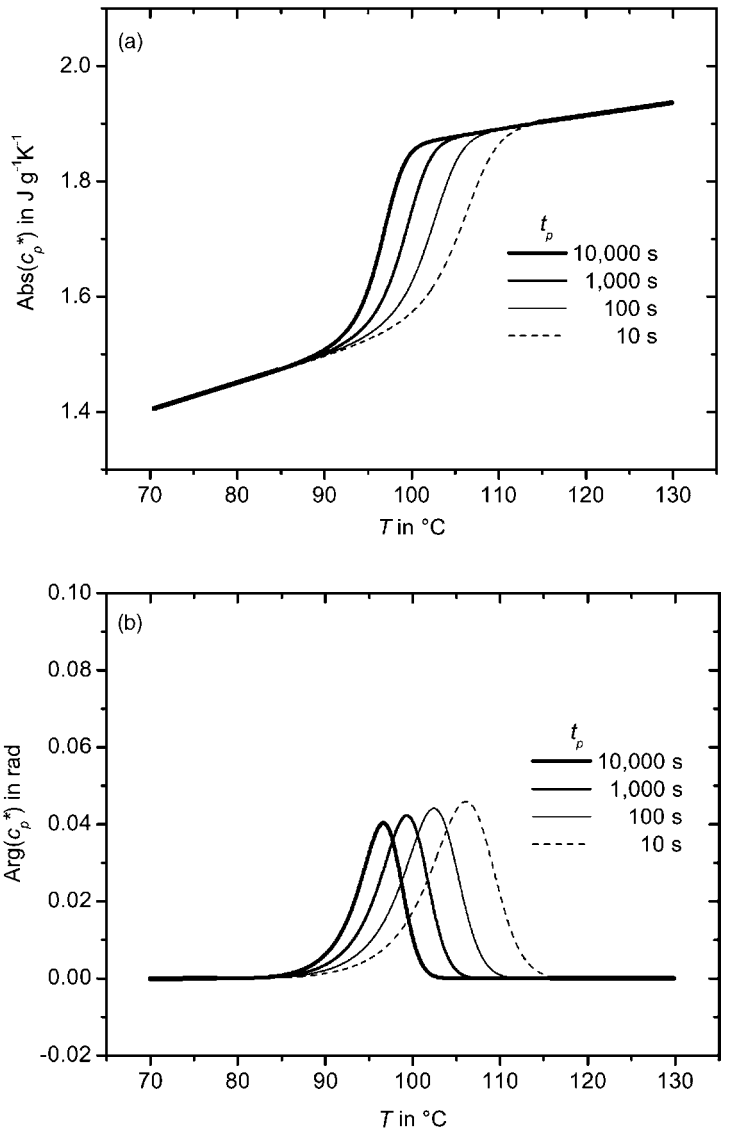

Fig. 1. Calculated magnitude (a) and argument (phase angle, b) of the complex heat capacity $C_p^*(T)$ of PS for different modulation periods t_p (see [2]).

algorithm—deviated (even partly) more than those limits was taken as unusable frequency for that calibration algorithm.[2]

[2] In reality we compared the magnitude of effective heat capacity C_{eff}^* outside the transition at higher frequencies with the value at the lowest frequency rather than with the absolute value from literature. This way possible systematic uncertainties, due to wrong heat flow calibration of our DSC, were disregarded.

2. Calibration examples

2.1. Results without any calibration

The uncorrected results (raw data) of C_{eff}^* (from sample plus pan) for the glass transition region of PS are shown in Fig. 2.

Taking our criterion into account one could, in this case (and with this DSC), measure the amplitude with

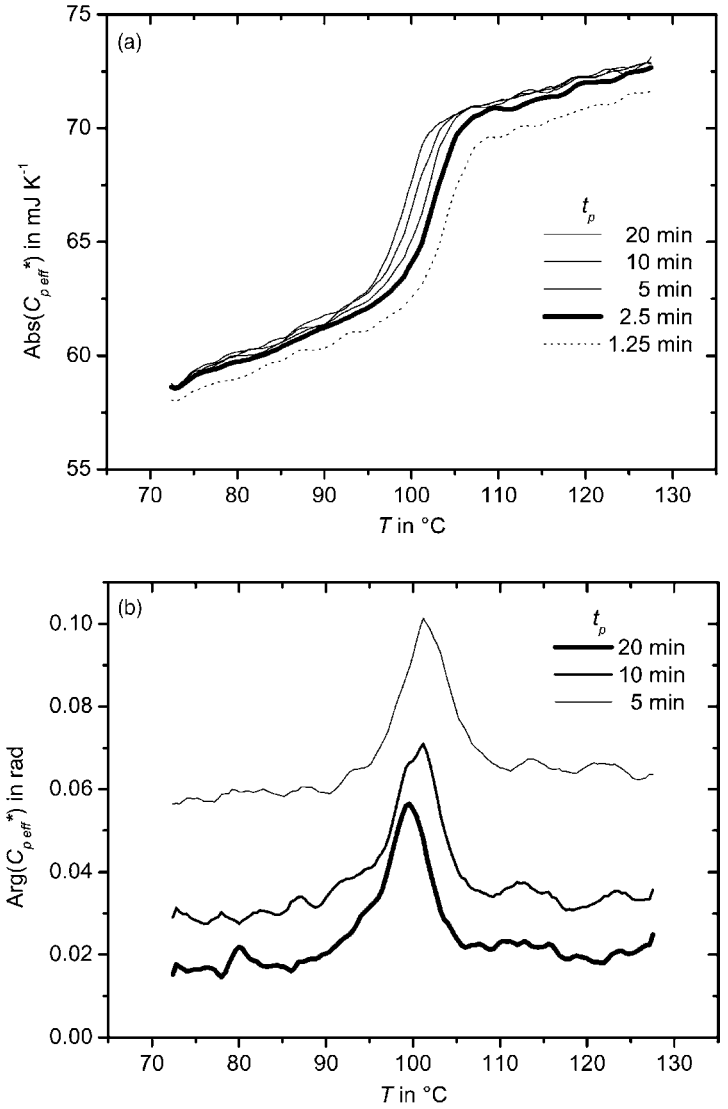

Fig. 2. Measured raw data of magnitude (a) and phase angle (b) of effective complex heat capacity C^*_{eff} of PS (25 mg) in Al pan (25 mg) vs. temperature for different modulation periods t_p. Perkin Elmer Instruments Pyris 1 DSC.

useful uncertainty at modulation periods down to 2.5 min, but for this period C^*_{eff} is already systematically somewhat too low. For the phase angle, on the other hand, one only obtains acceptable results at modulation periods of 20 min. In other words, modulation periods should be longer than 20 min to get correct phase angle without any calibration. This is nearly one order of magnitude more than for the magnitude measurement. For shorter periods a calibration method must be applied.

2.2. Results from "first order" calibration

If we want to perform the simple calibration procedure presented in Section 3.1 in [1], we have to compare the measured heat capacity outside the transition region with the true value and to determine some complex calibration factor, which depends on frequency and corresponds to the transfer function of the apparatus and sample system for the temperature in question. The simple calibration procedure assumes this factor to be

the same even for other temperatures and the region of transition as well and means the multiplication of the total measured C^*_{eff} with this factor.

Multiplication of a complex function with a complex factor means the multiplication of the magnitude with the absolute value of the calibration factor and the addition of the argument of that factor to the phase angle. Actually, we have (i) to multiply the Abs(C^*_{eff}) curve at each frequency with a proper factor to give the right value at some temperature outside the transition (in our example at 130 °C) and (ii) to shift the Arg(C^*_{eff}) curve vertically so that it becomes zero at the reference temperature outside the transition (e.g. at 130 °C), because the heat capacity is real valued there (no phase shift). The results of such a calibration algorithm are shown in Fig. 3.

With our quality criterion in mind we find from these results that the value of the Abs(C^*_{eff}) curve with

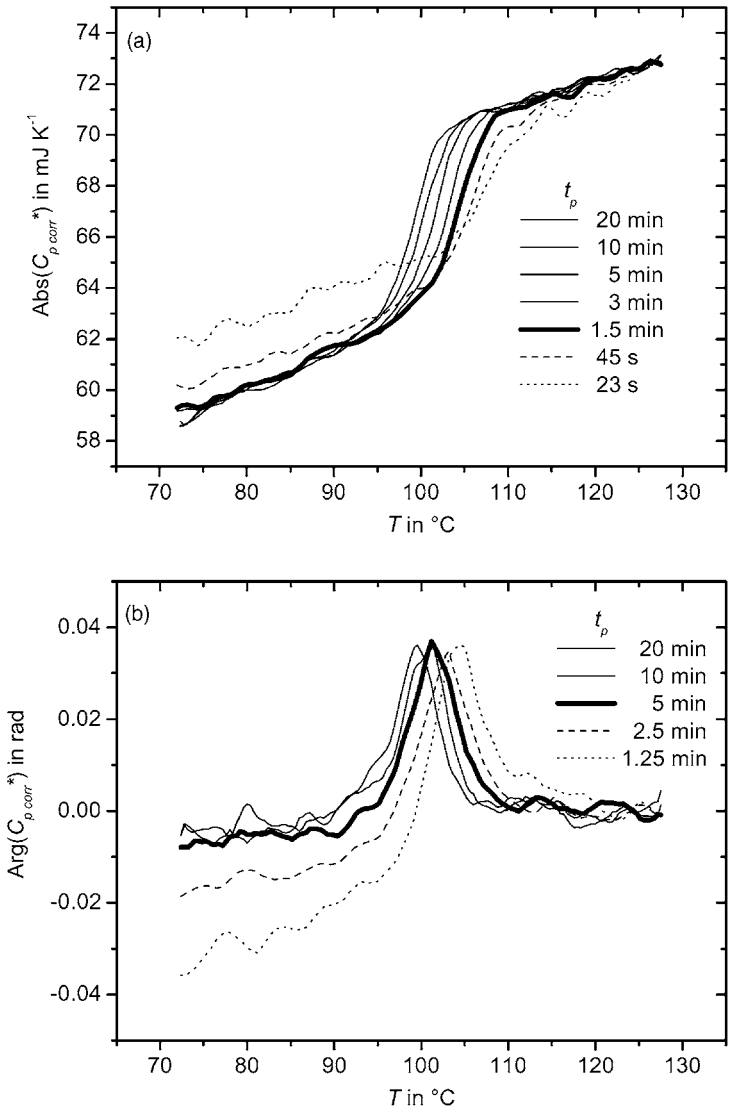

Fig. 3. "First order" corrected magnitude (a) and phase angle (b) of effective complex heat capacity C^*_{eff} (data from Fig. 2) vs. temperature for different modulation periods t_p.

45 s modulation period does not satisfy our condition below the glass transition region. Consequently, this calibration algorithm works well for Abs(C^*_{eff}) down to a modulation period of 1.5 min. The phase angle Arg(C^*_{eff}) does not satisfy our criterion at the modulation period of 2.5 min for lower temperatures, whereas the phase angle calibration works well down to a period of 5 min in this case.

2.3. Results from "second order" calibration

This improved calibration procedure does not use only one calibration factor for all temperatures, but starts from the fact that this factor could change with temperature. One way is to determine the transfer function on both sides outside the transition. In our example, we determined the transfer functions at about 70 and 130 °C. They turned out to be different and we get two different complex calibration factors at 70 and 130 °C. If one assumes a linear temperature dependence of the calibration factor in the temperature range 70–130 °C one has (i) to multiply the Abs(C^*_{eff}) curve of each frequency by a factor which changes linearly (i.e. a straight line) so that all curves coincide at the two reference temperatures below and above the transition region (in our example at 70 and 130 °C) and (ii) to subtract from Arg(C^*_{eff}) curve of each frequency a straight line so that the resulting curves are zero at those temperatures (i.e. at 70 and 130 °C) because C_p is real valued there. This type of phase angle calibration is used in the Perkin Elmer Instruments DDSC™ software. The results of such a calibration are shown in Fig. 4.

As can be seen, the value of Abs(C^*_{eff}) below glass transition region at 45 s modulation period is now in good agreement with the values at longer periods, but deviations remain just above the glass transition. In the temperature region 110–115 °C the Abs(C^*_{eff}) curve at 45 s does not satisfy our criterion. Therefore, the "second order" calibration algorithm applied to the magnitude (using two reference temperatures above and below the transition) yields only a minor improvement in comparison to the "first order" calibration. The respective phase angle calibration works well down to a modulation period of 3 min. At 1.5 min and shorter periods a tendency of the measured phase angle (Arg(C^*_{eff}) curves) to be much above the expected value is clearly visible for temperatures above the glass transition.

So far the methods presented in Sections 3.1 and 3.3 in [1] can be used to determine the calibration function (i.e. the reciprocal transfer function) for the "first" or "second order" calibration. Wunderlich and co-workers [4,5] introduced an effective time constant to describe the frequency dependence of the measured apparent heat capacity in a temperature region where the sample heat capacity is frequency independent (see Section 3.2 in [1]). By extrapolation of $1/c_p^2$ over ω^2 against $\omega \to 0$, in other words, using this time constant approach, they corrected the measured c_p values outside as well as inside the transition region. This calibration procedure is essential the same as to determine the total transfer function of the apparatus and sample system with the restriction that in [5] only the magnitude (absolute value) calibration is discussed, because the authors limit themselves to static heat capacity determinations. However, the calibration algorithm they recommend works similar both for "first order" and "second order" calibrations, depending on whether one uses only one or both temperature regions outside the transition in question.

To improve the "second order" calibration algorithm presented, one has to make further assumptions how the transfer function may depend on temperature and/or on sample properties. Weyer et al. [6], for example, discussed in detail the wrong phase angle calibration (the overestimated values above the glass transition at 1.5 min and 45 s periods of Fig. 4). They assumed that the phase lag φ due to heat transfer can be described as $\varphi = \omega \mathrm{Abs}(C^*_{\mathrm{eff}})/K$, with ω the angular frequency of temperature modulation and K the thermal contact between the sample and the aluminum pan. They presented an improved "second order" phase angle calibration algorithm by subtracting not a straight line but some curve proportional to the measured heat capacity, i.e. Abs(C^*_{eff}), from the measured phase angle in that region. Provided the thermal contact between sample and pan is kept constant (e.g. by using silicon oil as contact medium) such a correction works well down to a modulation period of 1 min.

It should be emphasized that the thermal contact changes with temperature (in particular during transitions) in a generally unknown manner. Additionally, the measured phase angle contains contributions from the instrument as well.

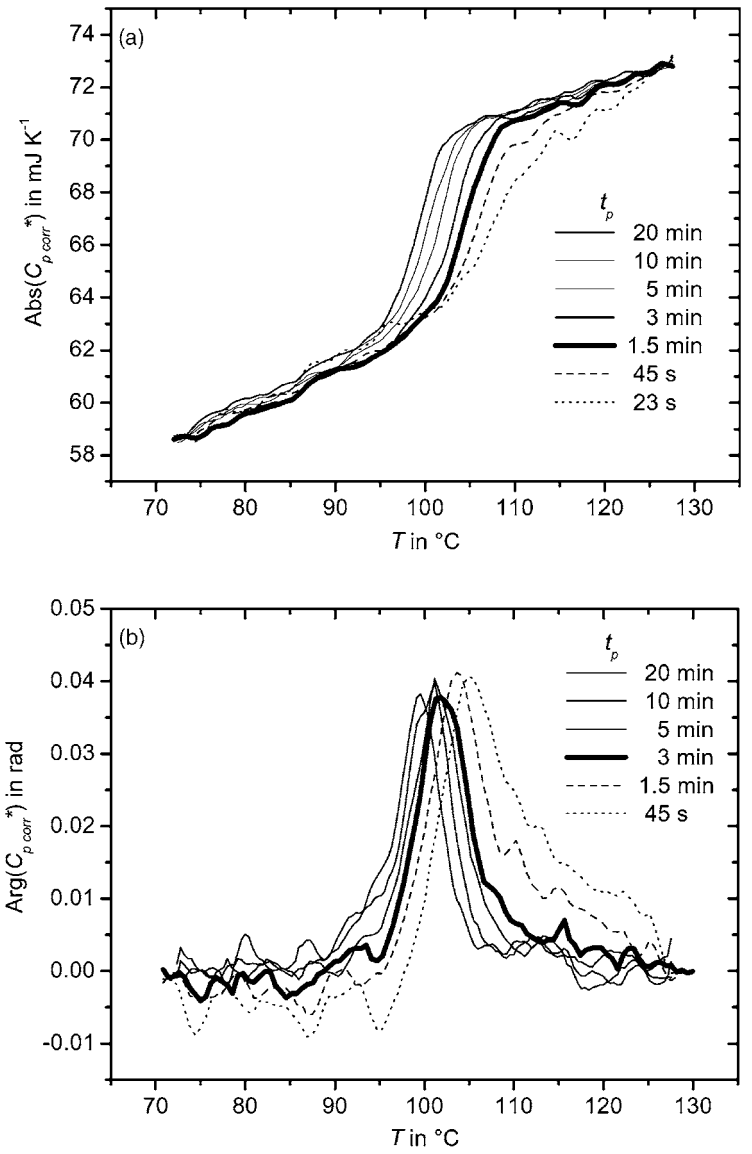

Fig. 4. "Second order" corrected magnitude (a) and phase angle (b) of effective complex heat capacity C^*_{eff} (data from Fig. 2) vs. temperature for different modulation periods t_p.

2.4. "Third order" calibration

As stated before, the total transfer function (apparatus and sample system) is a product of the transfer functions of its elements (see Section 1 in [1]). In other words, the (complex) total calibration factor, the reciprocal of the transfer function, can also be taken as a product of the calibration factors of its separate parts. Here we consider the total calibration factor $B^*(\omega, C^*_p(\omega), K, \ldots)$ (depending on frequency ω and all sample parameters including heat capacity $C^*_p(\omega)$, thermal contacts K, etc.) as a product of two factors: one factor $B^*_1(C^*_p(\omega), K, \ldots)$ depending on sample parameters stands for the sample influence, and another factor $B^*_2(\omega)$, which depends only on frequency (and of course on temperature) describing

the influence of the apparatus on the measured quantity:

$$B^*(\omega, C_p^*(\omega), K, \ldots) = B_1^*(\omega, C_p^*(\omega), K, \ldots) \cdot B_2^*(\omega) \quad (1)$$

In Section 3.4 in [1] it is described how to determine $B_2^*(\omega)$, the apparatus calibration function. It includes the dynamic response of the instrument (and software filtering, sampling rate and so on). It can be determined in advance and can be used for all further measurements provided that the instrumental settings are kept the same.

The first step of the calibration algorithm is to correct the measured (non-calibrated) effective heat capacity $C_{\text{eff}}^*(\omega)$ for the instrument dynamic response: $C_{\text{eff}}^*(\omega) \cdot B_2^*(\omega) = C_\beta^*(\omega)$. This results in $C_\beta^*(\omega)$, the actual apparent heat capacity of the sample as seen by the instrument from the furnace. It is shown in Section 3.4 in [1] that the sample itself behaves like a simple *RC*-element. This means that

$$C_\beta^*(\omega) = \frac{C_p(\omega)}{1 - (i\omega C_p(\omega))/K} \quad (2)$$

For those temperatures where the sample heat capacity is frequency independent the magnitude should read:

$$\left|C_\beta^*(\omega)\right| = \frac{C_p}{\sqrt{1 + (\omega C_p/K)^2}} \quad (3)$$

with K effective thermal contact and $C_p^*(\omega)$ the net heat capacity of the sample and the aluminum pan. From that follows: if we plot $1/\left|C_\beta^*(\omega)\right|^2$ for different frequencies versus ω^2 the points should lie on a straight line and the slope of the curve should equal $1/K^2$. If the unit of $\left|C_\beta^*(\omega)\right|$ is J K^{-1} and that of ω is rad s^{-1} then the effective thermal contact K will read in W K^{-1}. From Fig. 5 it is clear that for our sample the approach with one effective thermal contact holds up to $\omega^2 = 0.08$ rad^2 s^{-2} (which equals a period $t_p = 23$ s). At higher frequencies the measured values deviate downward from the straight line showing the increasing influence of the thermal conductivity of the sample itself.

Calculating such curves in dependence on temperature we are able to determine the effective thermal contact K between the sample and the instruments from the respective slopes as a function of temperature (see Fig. 6).

In the glass transition region the sample heat capacity depends on frequency, K is not determined correctly there and we have to interpolate the correct K value in the glass transition region from the values outside of it (dotted line in Fig. 6). It is obvious that the thermal contact is not a constant but increases with temperature above the glass transition region.

The second step of the calibration algorithm is to correct for the sample dynamic response, but it is not

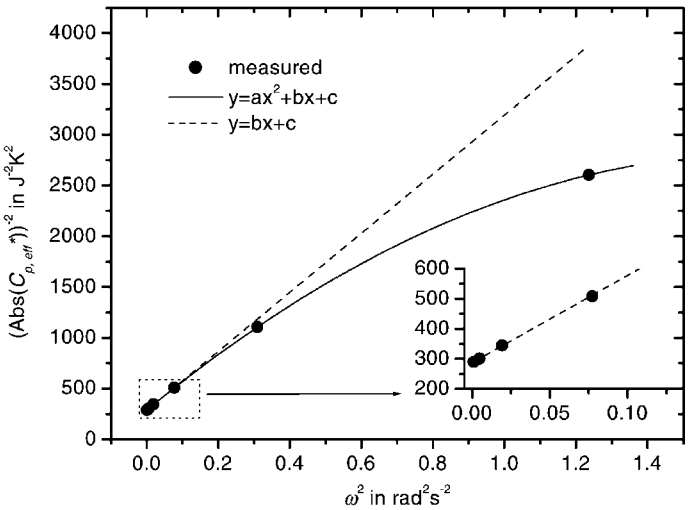

Fig. 5. Squared reciprocal magnitude of $C_\beta^*(\omega)$ vs. squared angular frequency (inset: linear behavior in the low frequency region).

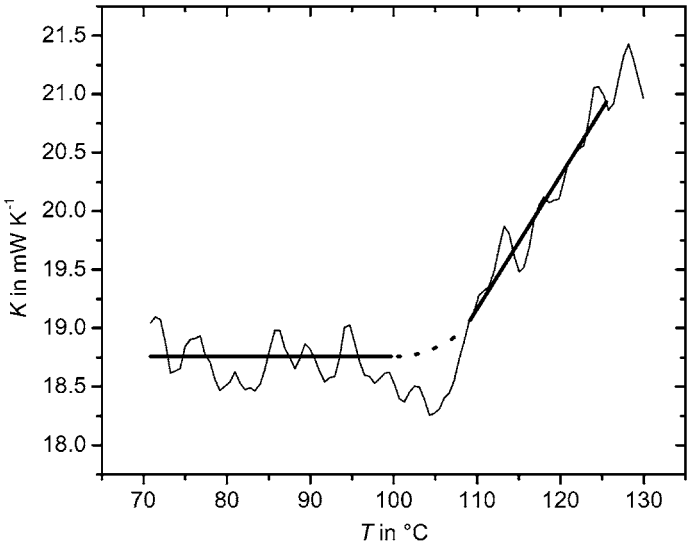

Fig. 6. Effective thermal contact K vs. temperature. The thin line gives the measured values from the slope of curves (like in Fig. 5) determined at all temperatures. The thick line is the fit function used for calibration. In the glass transition region this function has to be interpolated (dotted line).

necessary to determine $B_1^*(\omega, C_p^*(\omega), K, \ldots)$ explicitly. Because Eq. (2) is valid for complex $C_p^*(\omega)$ we can rearrange it to get $C_p^*(\omega)$:

$$C_p^*(\omega) = \frac{C_\beta^*(\omega)}{1 + (i\omega C_\beta^*(\omega))/K} \tag{4}$$

With the (known) heat capacity of the sample pan one can calculate the corrected complex specific heat capacity of the PS sample:

$$c_p^*(\omega) = \frac{(C_p^*(\omega) - C_{p,\mathrm{pan}})}{m_{\mathrm{sample}}} \tag{5}$$

with $C_{p,\mathrm{pan}}$ the heat capacity of the (aluminum) pan and m_{sample} the sample mass. The results of these calculations are shown in Fig. 7. Obviously the calibration algorithm works both for the magnitude and for the phase angle for modulation periods down to 45 s. If we want correct results for higher frequencies (smaller periods) we have to take the thermal conductivity of the sample into account too. An interesting point to note is that the curves with 23 and 12 s periods do not change the shape compared to the curves at longer periods.

As this example shows, the period range resulting in correct values is not much larger for the third order calibration than for the simpler methods. It is, however, the only method which allows to determine the change of the transfer function during the measurement, in particular even for the transition region. Of course, the modulation form of choice should be one to get a multi-frequency response: the temperature-step (periodic or non-periodic) method or any periodic non-sinusoidal temperature modulation method.

2.4.1. Remark concerning small samples

The problems resulting from heat transfer can be minimized by using very small samples (and very small sample pans as well) for the measurements. We performed such a measurement with a 2 mg PS sample wrapped in an aluminum foil of 2 mg. The sample was very thin and flat with the same diameter as the standard aluminum pans. The results from the measurements using a "second order" calibration algorithm are shown in Fig. 8.

In this case the curves coincide, within the limits of experimental uncertainties, down to modulation periods of 7.5 s. Nevertheless, it is difficult to make a quantitative analysis with these data because of the poor quality. Larger samples will, of course, result in a better signal-to-noise ratio but at the expense of falsified heat capacity curves because of the heat transfer influence.

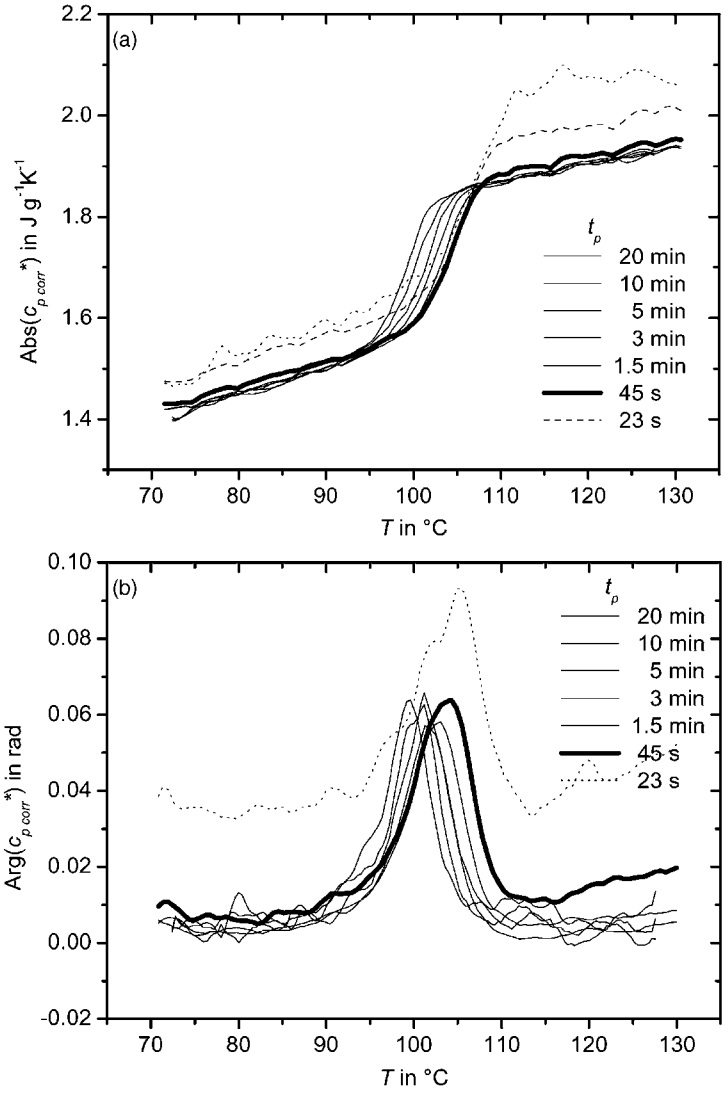

Fig. 7. "Third order" corrected magnitude (a) and phase angle (b) of complex specific heat capacity c_p^* (data from Fig. 2) vs. temperature for different periods t_p.

It is a matter of experience to find the right balance between the uncertainties caused by a low signal-to-noise ratio and those from a faulty correction because of the sample heat transfer influence.

3. Conclusions

It has been shown that there are different possibilities to calibrate the TMDSC for heat transfer influences. For common purposes, in particular if it is sufficient to correct the magnitude of the (complex) apparent heat capacity and disregard the phase angle, one can use the known heat capacity of the sample (in temperature regions outside of reactions or transitions) as an internal reference and correct the measured values correspondingly.

Multi-frequency measuring methods offer the possibility to get the frequency dependence of the measured heat capacity at a certain moment from one

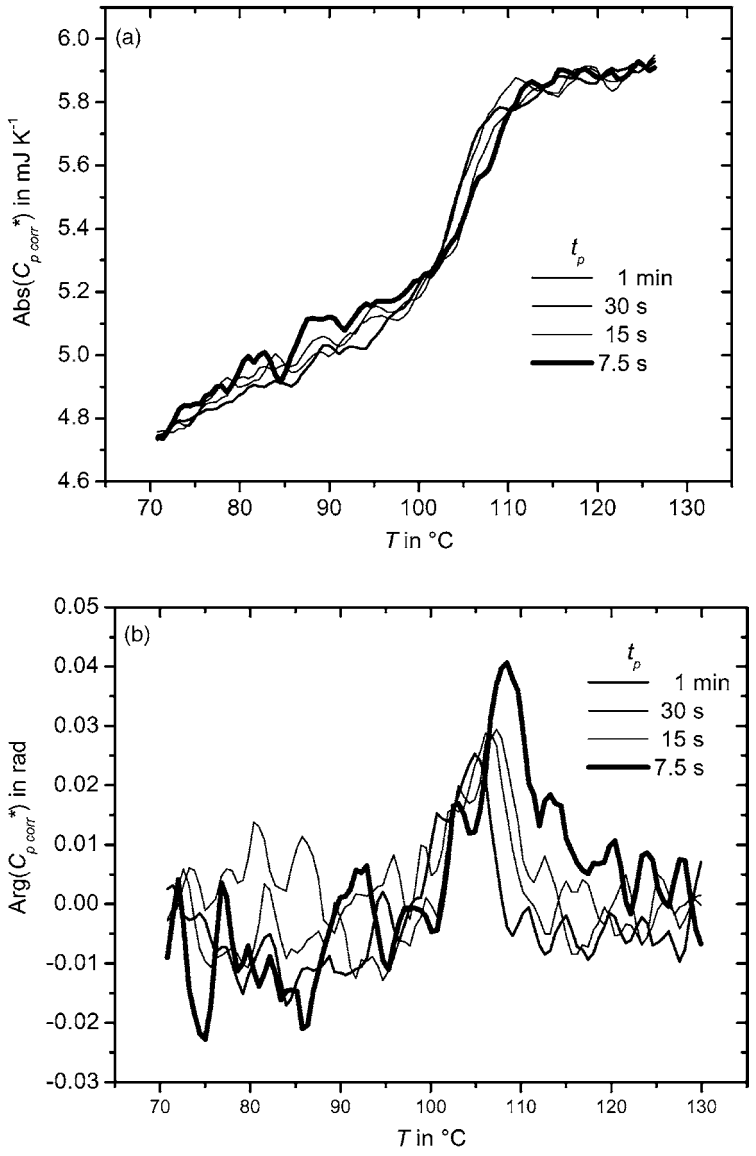

Fig. 8. "Second order" corrected magnitude (a) and phase angle (b) of effective complex heat capacity C^*_{eff} of a small PS sample ($m_{\mathrm{s}} = 2$ mg) in Al foil ($m_{\mathrm{Al}} = 2$ mg) vs. temperature for different modulation periods t_p.

single measurement. This allows, in temperature regions where the sample heat capacity is frequency independent, to extrapolate the measured quantity to zero frequency to get the correct heat capacity value.

In cases where the complex heat capacity is of interest (e.g. for transitions), both magnitude and phase angle must be corrected. To get a detailed insight into the heat transfer behavior of the DSC as well as the sample itself, the advanced calibration procedure is recommended (see Section 3.4 in [1]) which allows to separate between the influences of the apparatus and the sample as well as to determine the change of the transfer function during the measurement. This method is somewhat more time consuming, but seems to work successfully even for the transition region and leads to more certain results.

The example has shown that the more simple calibration procedures lead to nearly the same uncertainties of the results in everyday measurements as the more sophisticated "third order" calibration procedure does. We recommend, however, the "third order" calibration procedure in all cases where the heat transfer conditions could change during the measurement.

Acknowledgements

This research was supported by the German Science Foundation (Grant DFG Schi-331/5-1). MM acknowledges support by Perkin Elmer Instruments.

References

[1] G.W.H. Höhne, M. Merzlyakov, C. Schick, Calibration of magnitude and phase angle of a TMDSC signal. Part 1. Basic considerations, Thermochim. Acta 391 (2002) 51–67.
[2] S. Weyer, M. Merzlyakov, C. Schick, Thermochim. Acta 377 (2001) 85–96.
[3] M. Merzlyakov, C. Schick, Thermochim. Acta 377 (2001) 193–204.
[4] R. Androsch, B. Wunderlich, Thermochim. Acta 333 (1999) 27–32.
[5] R. Androsch, I. Moon, S. Kreitmeier, B. Wunderlich, Thermochim. Acta 357 (2000) 267–278.
[6] S. Weyer, A. Hensel, C. Schick, Thermochim. Acta 304/305 (1997) 267–275.